Characterization of soft x-ray critical-angle transmission gratings for the REDSoX polarimetry sounding rocket

Ralf K. Heilmann^a, Alexander R. Bruccoleri^b, Alan Garner^c, Eric M. Gullikson^d, Hans M. Günther^c, Sarah N. T. Heine^c, Herman L. Marshall^c, and Mark L. Schattenburg^a

aSpace Nanotechnology Laboratory, MIT Kavli Institute for Astrophysics and Space Research, Massachusetts Institute of Technology, Cambridge, MA 02139, USA
bIzentis, LLC, Cambridge, MA 02139, USA
dLawrence Berkeley National Laboratory, Berkeley, CA 94720, USA
cMIT Kavli Institute for Astrophysics and Space Research, Massachusetts Institute of Technology, Cambridge, MA 02139, USA

ABSTRACT

The Rocket Experiment Demonstration of a Soft X-ray Polarimeter (REDSoX) is a sounding rocket instrument that was selected by NASA to make the first measurement of the linear X-ray polarization of an astrophysical source in the 0.2-0.4 keV band. The optical design employs Wolter-I focusing mirrors, followed by critical-angle transmission (CAT) gratings to disperse x rays onto dispersion-matched laterally-graded mulitlayers, which in turn reflect x rays near the Brewster angle for a broadband, polarization-sensitive response.

The instrument contains three parallel channels with 120 degree azimuthal rotation between them to achieve polarization modulation factors over 90%. About 50 CAT gratings ($\sim 38 \times 11~\mathrm{mm}^2$ each) are being fabricated to cover the required aperture. Over 40 gratings have been produced to date and are at various stages of metrology and characterization. Here we present our methods and the current status. CAT gratings feature 200 nm-period, freestanding, ultra-high aspect ratio grating bars. They are fabricated from 200 mm silicon-on-insulator wafers using optical projection lithography, deep reactive-ion etching, KOH polishing, critical-point drying, and oxide removal via HF vapor. Grating bar tilt is measured using small-angle x-ray scattering and used for grating alignment. Diffraction efficiency performance in the soft x-ray band is characterized on our in-house beamline.

We also present recent diffraction efficiency improvements for deeper CAT gratings with reduced support structure blockage.

Keywords: REDSoX, critical-angle transmission grating, x-ray polarimetry, blazed transmission grating, soft x ray

1. INTRODUCTION

The Rocket Experiment Demonstration of a Soft X-ray Polarimeter (the REDSoX Polarimeter) is designed to measure linear x-ray polarization from astrophysical objects in the soft x-ray band below 1 keV. It was selected by NASA and is scheduled to launch in late 2027. REDSoX is complementary to the Imaging X-ray Polarimetry Explorer (IXPE), which has sensitivity only above 2 keV. A prime example for soft x-ray spectropolarimetry would be sources such as isolated neutron stars and their magnetized atmospheres, which are detectable primarily below 1 keV.

However, for the first flight the observation target is the blazar Mrk 421, currently the brightest active galaxy. It contains parsec-scale jets with $\beta = v/c \sim 0.995$ or higher, with a potential maximum polarization fraction P_{max} of 79% for a model with simple, uniformly magnetized X-ray emission regions. Jet and shock models predict different magnetic field orientations, and different outcomes for P_{max} would help to distinguish between different scenarios.³

Further author information: (Send correspondence to R.K.H.) E-mail: ralf at space.mit.edu, URL: http://snl.mit.edu/

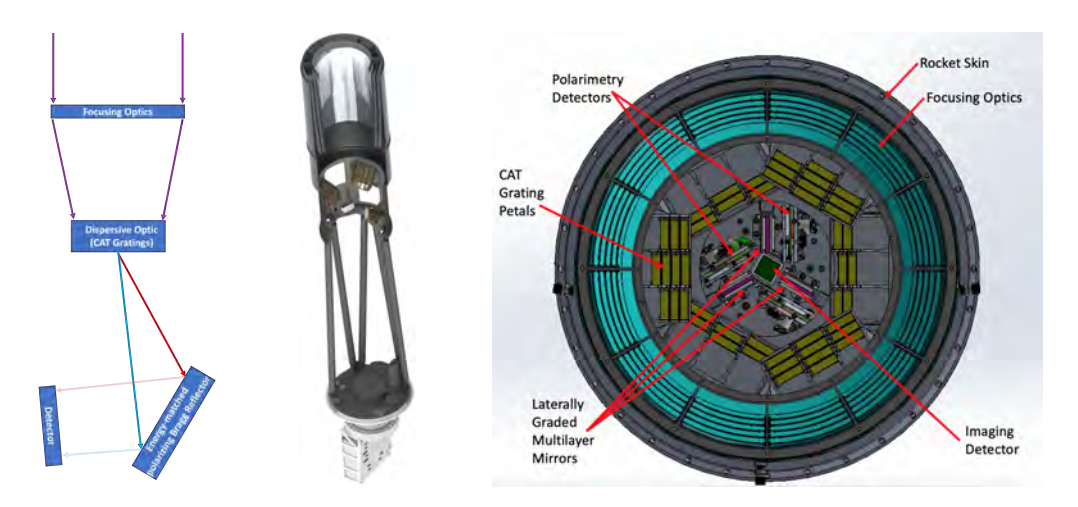


Figure 1: Left: Simplified REDSoX optical design concept. Middle: CAD rendering of a recent mechanical design. Right: Most recent CAD model, looking towards the mirror focus along the optical axis. Each channel has ten gratings closer to the mirrors (e.g., grating petal at the 9 o'clock position) and six gratings closer to the focal plane (e.g., petal at the 3 o'clock position), with the blazed first order from both petals landing on a single LGML (e.g., 12 o'clock position).

The optical design (see Fig. 1) features full-shell, replicated nickel Wolter-I mirrors with 2.5 m focal length from NASA's Marshall Space Flight Center. The mirror module contains five full shells and will have an angular resolution of ≤ 30 arcsec half power diameter (HPD).⁴

Critical-angle transmission (CAT) gratings are inserted into the converging beam in three optical channels, rotated around the optical axis by 120 degrees relative to each other. Each channel contains gratings that cover two roughly 60 degree azimuthal sub-apertures across from each other. The sub-apertured point-spread function (PSF) will have a reduced width around 10 arcsec (full-width half-max, FWHM) in 1-D (along the grating dispersion direction).

The grating dispersion and the peak reflectivity of a downstream laterally-graded multilayer mirror (LGML, made by E.M.G., Lawrence Berkeley National Lab (LBNL)) must be made to match to generate a broad-band instrument response. This results in a stair-stepped design with gratings that are wide in the dispersion direction and narrow in the cross-dispersion direction.^{1,5} The incidence angles onto the LGMLs are near 45 degrees, which is near the polarization-sensitive Brewster angle. After reflection the beams are read out with commercial CCDs (one per channel). Direct (undiffracted, 0^{th} order) beam photons create an image at the focus of the mirror assembly, where a fourth CCD is located. More details can be found in References 1 and 3. For the rest of this work we focus on the diffraction gratings.

For soft x-ray diffraction gratings, several grating choices are available, such as transmission and in-plane and off-plane reflection gratings.⁶ Apart from performance, cost and easy availability are a major concern for a low-budget sounding rocket project. Transmission gratings operate near normal incidence and therefore require the least geometric area to cover a given telescope aperture. They have the added advantages of low mass due to their thinness, and - due to the transmission geometry - relaxed alignment tolerances compared to reflection gratings.

In the 0.2 - 0.4 keV soft x-ray band high diffraction efficiency is difficult to achieve. The grating support membranes in gratings such as the ones on the Chandra HETGS⁷ absorb too many soft x rays, leading to first-order efficiencies below 3%. Freestanding gratings require cross support structures that block x rays, such as the LETG on Chandra. Except for very small depths on the order of a few hundred nanometers or less, grating bars are opaque to soft x rays, resulting in an amplitude grating with maximum first-order efficiency of 10% before taking support structure blockage into account. A very thin grating that acts as a phase-shifting grating could achieve on the order of 11-12% (250 nm of Si) or $\sim 15-19\%$ (350 nm of Be) over the 0.2 - 0.4 keV band,

but would be extremely difficult to fabricate without an absorbing support membrane, especially over hundreds of square centimeters.

For REDSoX the choice was made to use CAT gratings, which offer all the advantages of transmission gratings, plus the potential use of diffraction orders higher than first with higher efficiency and resolving power. However, for various reasons, we decided to use CAT gratings in first order in this first implementation of REDSoX, where we typically find diffraction efficiency in the 10-15% range, averaged over the whole grating area, and including blockage from support structures. Another reason for choosing CAT gratings was the geographic proximity of in-house CAT grating expertise, development and fabrication, and opportunities for cost-saving synergy with the ongoing research efforts at the MIT Space Nanotechnology Laboratory, such as the sharing of wafer runs at MIT Lincoln Laboratory.

Up to now CAT gratings have only been made in relatively small numbers for technology demonstration and testing purposes. This is the first time that a larger number of exchangeable CAT gratings are fabricated for a flight program, which provides a valuable learning opportunity for potential future, larger flight programs that require hundreds to possibly thousands of high-quality CAT gratings. $^{10-12}$ For the latest REDSoX design, 48 gratings (16 per channel) of size 38×10.75 mm² are required, plus spares.

In the following we briefly describe how CAT gratings work and how they are fabricated. We then discuss certain aspects of grating fabrication and metrology, focusing on the problem of bar tilt variations, and how metrology, efficiency modeling, and ray tracing work together to predict grating performance, and how results influence logistics and tool choices.

We then discuss soft x-ray diffraction efficiency measurements at the MIT polarimetry beamline and the first "CAT grating rocket flight", followed by a brief update on CAT grating development beyond REDSoX.

2. CAT GRATING DESIGN AND FABRICATION

CAT gratings are blazed transmission gratings. They feature ultra-high aspect-ratio, freestanding grating bars with nm-smooth sidewalls.¹³ The entire grating is inclined such that x rays of wavelength λ impinge on the grating bar sidewalls at graze angles θ below the critical angle for total external reflection θ_c (see Fig. 2). Diffracted orders around the direction of specular reflection from the nm-smooth sidewalls are strongly enhanced ("blazed"). This allows the use of higher orders for higher spectral resolving power $R = \lambda/\Delta\lambda$ on the order of 10^3 to 10^4 , depending on the spectrometer design. For REDSoX, such high R is not required. Instead, we blaze for first order in the middle of the bandpass.

The diffraction angle β_m for the m^{th} diffraction order is given by the grating equation

$$\frac{m\lambda}{p} = \sin\theta - \sin\beta_m,\tag{1}$$

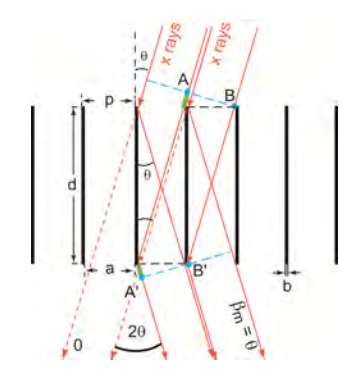
where p is the grating period. The small critical angles for soft x rays (typically on the order of 1-2 degrees) demand high-aspect ratio grating bars in order to intercept all incoming photons. Furthermore, we want the bars to be as thin as possible to minimize blockage and absorption.

CAT gratings were originally developed for applications with a broader bandpass ($\sim 0.2\text{-}1 \text{ keV}$) such as Arcus^{10,11} and Lynx.¹²

Here we use the Arcus design with grating period p=200 nm, grating bar depth d=4 micrometers, and bar thickness $b\approx 60$ nm. (Recently, we demonstrated $d>5.5~\mu\mathrm{m}.^{14}$) This allows us to benefit from the ongoing, separately funded research efforts on CAT gratings, for example by combining wafer production and patterning runs.

Blazing is most efficient when $\tan \theta \approx (p-b)/d$. For $d=4~\mu\mathrm{m}$ this means $\theta \approx 2$ degrees, but in the 0.2-0.4 keV range the gratings also work well in first order at lower blaze angle, even at the non-optimal depth of 4 $\mu\mathrm{m}$.

CAT grating bars are not supported by a membrane, but freestanding. As seen on the right in Fig. 2, the bars are held in place by a monolithically integrated 5 μ m-period Level 1 (L1) support mesh. Additional coarser and thicker support structures (Level 2/L2 hexagonal supports) are needed for the few- μ m thin grating layer in



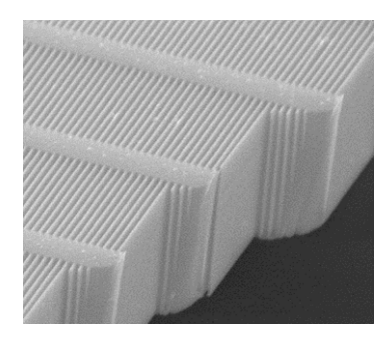


Figure 2: Left: Schematic cross-section through a CAT grating of period p. The m^{th} diffraction order occurs at an angle β_m where the path length difference between AA' and BB' is $m\lambda$. Shown is the case where β_m coincides with the direction of specular reflection from the grating bar sidewalls ($|\beta_m| = |\theta|$), i.e., blazing in the m^{th} order. Right: Scanning electron micrograph (SEM) of a cleaved CAT grating membrane showing top, cross-section and sidewall views of the 200 nm-period silicon grating bars and their monolithically integrated 5 μ m-period L1 cross supports (x rays enter from the top and leave out the bottom).

order to manufacture large enough individual CAT gratings such that a manageable number covers large areas on the order of thousands of square centimeters. For REDSoX we only need a few hundred square centimeters. Due to the stepped grating array design we use gratings about one third of the size developed for Arcus, namely $38 \times 10.75 \text{ mm}^2$.

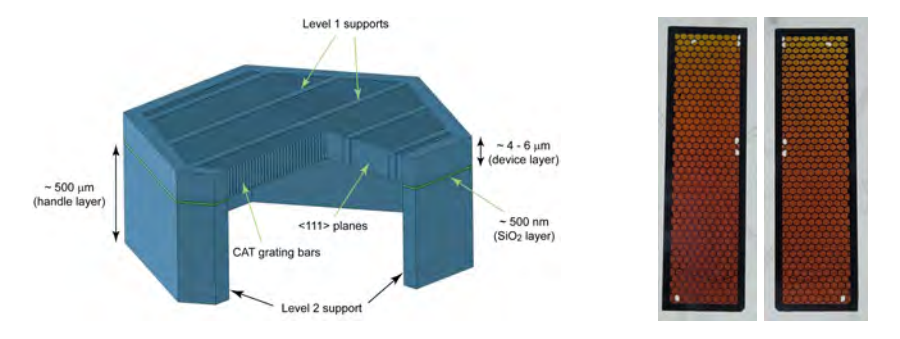


Figure 3: Left: Schematic showing the structural hierarchy of a CAT grating membrane (not to scale). Right: Photographs of front and back side of a representative 38 x 10.75 mm² REDSoX CAT grating membrane with back illumination to highlight the hexagonal L2 mesh. For this grating six out of its over 400 hexagons are damaged.

Fabrication has been described extensively in previous work.^{13,15-17} CAT gratings are currently produced from 200 mm enhanced silicon-on-insulator (E-SOI) wafers. The thin Si device ("front side") layer of the E-SOI wafer is manufactured to thickness d (see Fig. 2) within ≤ 100 nm thickness variation across the whole wafer. Using 193 nm 4X optical projection lithography (OPL) at MIT Lincoln Laboratory, patterns for CAT gratings, L1 and L2 structures are simultaneously transferred into a silicon oxide layer that serves as a mask for the subsequent key step that creates the ultra-high aspect-ratio grating bars: the front side deep reactive-ion etch (DRIE).

Before the front side DRIE we expose the resist on the ~ 0.6 mm thick handle ("back side") layer of the SOI wafer with an array of 36 1-mm-wide frames (L3) with the dimensions of an individual CAT grating, and with a hexagonal pattern that is aligned with the front side L2 hexagons. The developed combined pattern serves as a mask for an oxide etch. The resulting oxide pattern is later used as a mask for the back side DRIE step.

CAT gratings can be fabricated in volume manufacturing mode from 200 mm SOI wafers, ¹⁷ in principle

allowing for up to 36 REDSoX gratings to be produced from a single wafer (see Fig. 4). We were able to use a small number of 200 mm wafers that had their front sides etched on an advanced DRIE tool at the SPTS demonstration lab. These wafers became the prime choice for REDSoX gratings for reasons outlined in more detail below.

In general, for a rocket program we do not have access to dedicated 200 mm tools for every process step, and most tools that we can use are general user tools that are utilized by a variety of groups for a variety of purposes. Therefore, for any additional wafer we had to use DRIE tools with smaller chucks for the front side etch.

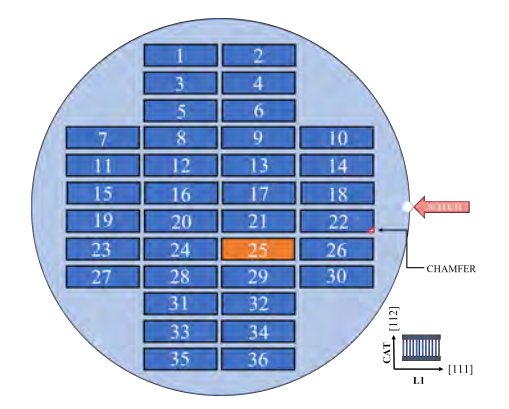
We cleave the 200 mm SOI wafer into individual REDSoX gratings and continue our work on smaller tools. Some of these are in the Space Nanotechnology Lab, some in MIT.nano, and some outside of MIT.

The grating bar patterns were aligned parallel to the vertical {111} planes of the (110) device layer during OPL. Since DRIE leaves rough sidewalls, this crystal orientation is used so we can "polish" the grating bar sidewalls post-DRIE through immersion in KOH solution.¹³ The gratings then have to be dried in a critical-point dryer (CPD) to prevent stiction from liquid-vapor surface tension.

The front side is then protected with a PECVD low-stress layer of tetraethyl orthosilicate (TEOS) and spunon ProTek, and bonded to a carrier wafer using Crystalbond. Now the grating is ready for back side DRIE. This step is mostly performed on a 150 mm tool at Harvard. This is followed by debonding from the carrier, piranha cleaning, and CPD.

Finally, the buried oxide layer separating device and handle layers is removed with an HF vapor etch in the areas not covered by Si, resulting in a monolithic Si grating layer with freestanding CAT grating bars, integrated L1 and L2 supports, and a bulky L2 mesh. This step is mostly performed on a Primaxx μ Etch tool at Cornell. The final product can be described as a perforated Si membrane of thickness d, backed by a 0.6 mm-thick hexagonal (L2) support mesh and bordered by a 1 mm wide (L3) frame. We often refer to it as a Si grating membrane, which can be bonded to other structures along the L3 frame.

Since we do not have full control over many of the tools that we are using, a certain amount of potential grating material has to be used as witness samples to verify proper tool performance on any given day.



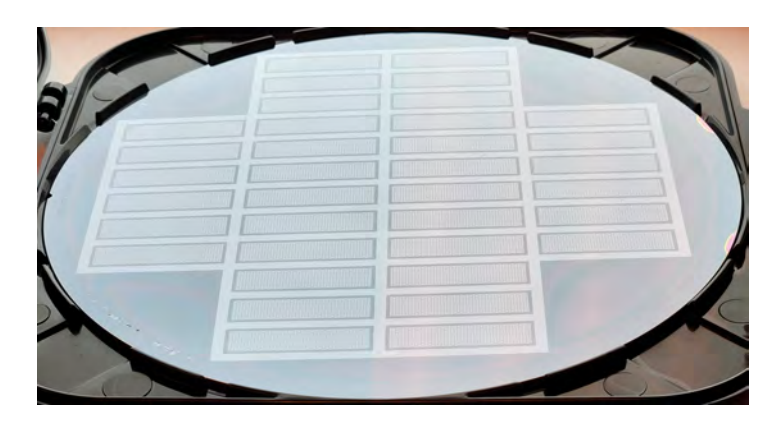


Figure 4: Left: Schematic of the 200 mm wafer backside map for REDSoX gratings. Section 25 is highlighted as an example. Right: Photograph of back side mask on a 200 mm SOI wafer, showing 36 grating sections with their 1 mm wide, rectangular 38×10.75 mm² L3 frames and hexagonal L2 mesh. Every L3 frame has a small diagonal chamfer in the same corner for orientation purposes.

Many considerations were taken into account before production could start. E-SOI wafers are long lead items, and LL wafer runs are not available on short notice on a small budget. Other decisions could be made later, such as the precise grating outer dimensions, since these can be easily customized with an on-campus laser writer. We highlight only a few considerations here.

A wafer run at LL can accommodate a batch of up to 25 200 mm wafers. Long before REDSoX grating production had been demonstrated, roughly half a batch was conservatively considered to provide enough patterned

wafers to safely last through production. This includes a certain amount of destructive testing to verify the quality of the produced structures at various steps. For example, in the initial stages one or more whole wafers have to be cleaved for diagnosis, which prevents the resulting fragements from being used without a carrier wafer for subsequent steps.

The width of the L3 frame was chosen to be only 1 mm, in contrast to 2 mm for the three times larger Arcus gratings. This makes handling of the gratings with tweezers much more difficult and more prone to damage, which mostly results in the loss of the device layer inside an individual L2 hexagon ("blown-out hexagon"). However, even if a few hexagons get blown out from handling, we are still gaining around 100 hexagons of useful grating area per grating by using the narrower L3 borders.

Fig. 5 shows 15 flight candidate gratings out of a batch of 25 after the final vapor HF step. Five more gratings from the same batch are considered lower quality backups, while another five were consumed as witness samples.

Starting with three and a half 200 mm wafers front side etched by SPTS (126 potential gratings), we currently expect to end up with about 75 flight-compatible gratings, resulting in an average yield of around 60% for the post-DRIE steps.



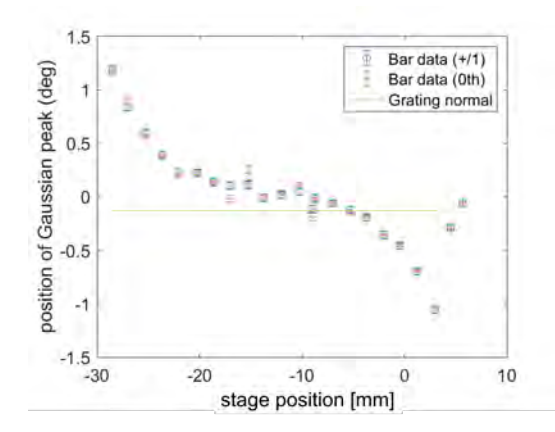
Figure 5: Photographs of 15 flight-quality REDSoX format CAT gratings from the most recent batch of 25.

3. GRATING BAR TILT AND SMALL-ANGLE X-RAY SCATTERING

Inhomogeneities in the various pattern transfer steps limit the use of the full wafer area. We observe some duty cycle (b/p) reduction in the oxide mask towards the wafer edge, which can lead to grating bars that are too thin to survive all the fabrication steps. A more significant effect is the fact that the front side DRIE does not etch perfectly parallel to the wafer surface normal, but changes the etch angle systematically by some amount across the wafer.¹⁸ The resulting so-called bar tilt leads to a variation in blaze angle, which must be measured and corrected for during grating alignment.¹⁹ In principle the bar tilt behavior can be influenced through DRIE tool recipe changes and/or chamber modifications, but systematic improvements would require feedback from fast inline metrology of bar tilt, which we are currently developing.²⁰ In the meantime, for REDSoX we simply have to accept the bar tilt variations that the tools we have access to provide, measure them, and align correspondingly.

We previously developed a method to precisely measure bar tilt using small-angle x-ray scattering (SAXS) with a Cu K_{α} source and laser reflection.²¹ For these measurements we do not need fully finished, freestanding gratings, but the wafer back side must at least be thinned to about 100 μ m for sufficient transmission. However, all data presented here was taken on finished, freestanding gratings.

The resulting bar tilt maps can then be used in conjunction with diffraction efficiency modeling to predict the efficiencies across each grating as a function of grating tilt. Fig. 6 shows two examples, one from a grating etched as a single chip, and one from a grating cleaved out of a wafer that was etched whole on a 200 mm tool. It is clear that full-wafer etching is preferred over chip etching.



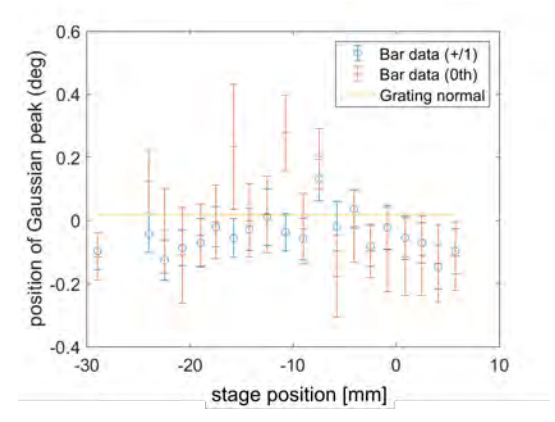


Figure 6: Relative bar tilt angle across a grating membrane derived from SAXS ($\lambda=0.154$ nm). The change in 0th or $\pm 1^{st}$ order diffraction efficiencies as a function of incidence angle is fitted to a Gaussian, and the peak position is plotted. The straight line is the angle of the grating surface normal measured via laser reflection. Left: Bar tilt for a grating that was front-side etched as a single grating-size chip bonded to a 150 mm carrier wafer (FL13). Clearly, the etch angle is strongly influenced by the substrate/sample inhomogeneities and height steps near the sample edges. Right: Bar tilt for a sample that was etched as a full 200 mm wafer as in Fig. 4 (FL15). The bar tilt variation around its average is minimal at around ± 0.1 deg. (The error bars for this data set are larger because a smaller, more collimated x-ray beam with lower flux was used without increasing the one second integration time per angle.)

4. DIFFRACTION EFFICIENCY MODELING

We model CAT grating diffraction efficiency using rigorous coupled-wave analysis (RCWA).²² The simplest model consists of grating bars with a rectangular profile defined by period p, depth d and width b (see Fig. 2). Real grating bars do not have perfectly rectangular profiles, but often show slow width variations from top to bottom in SEMs from cleaved cross sections. Analysis of synchrotron data and AFM show typical sidewall roughness on the order of 2-3 nm rms. We have achieved reasonable x-ray data fitting in the past with simple model bar profiles and a Debye-Waller-type roughness factor.¹⁷

For synchrotron data, which averages over a few hundred L1 periods, we model the effect of the L1 cross supports simply as a Si film of an area fraction derived from SEM images, where any partial transmission ends up in 0th order. For fully illuminated gratings we also multiply the predicted efficiency by the open area fraction of the L2 mesh, which is lithographically defined as 0.81 for all the gratings considered here. Fig. 7 shows RCWA predictions for two example models with different bar widths. Combining efficiency models with bar tilt data from SAXS, it is straightforward to estimate the diffraction efficiency across a given grating as a function of grating tilt and to provide useful input for the best tilt angle for each grating during alignment in the REDSoX grating array.

5. RAY-TRACING OF BAR TILT VARIATIONS

The REDSoX optical design has been continuously refined with the use of ray-tracing over the years.⁵ Here we model the impact that bar tilt variations across individual gratings have on the REDSoX modulation factor and effective area.

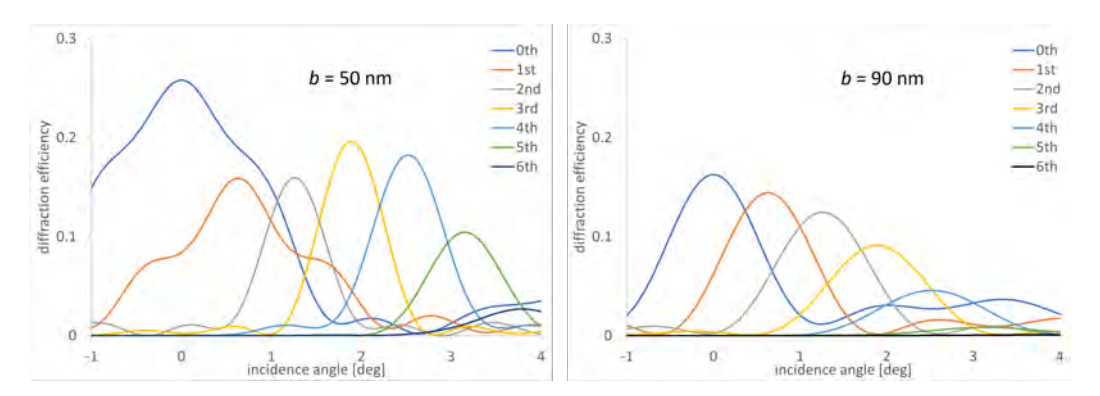


Figure 7: Example diffraction efficiencies predicted for a simple model with $d=4~\mu\text{m}$, p=200~nm, and $\lambda=4.4~\text{nm}$. Results were multiplied by 0.81×0.78 to take absorption by L1 and L2 supports into account. Left: Narrow bars with b=50~nm. Right: Wide bars with b=90~nm.

From previous studies, we know that bar tilt variations over a limited substrate distance can be approximated well by a linear change, as long as one stays sufficiently far away from wafer or chip boundaries (see also Fig. 6). 14, 18, 21, 23 For the results below, we assume that the average bar tilt across 36 mm of grating length is known from measurements, and that the grating is aligned with the average bar tilt vector at the design blaze angle relative to the convergent incident x-ray beam. Without loss of generality, the ray trace simply assumes that the grating bar tilt in the grating center is zero - meaning that the bars are perpendicular to the grating membrane surface. If the measured value is different from zero, we can mount the CAT grating holder at a slight angle to correct for that. In this case the membrane will not end up exactly at the ideal location and orientation, but the deviation is a second order effect that we can safely ignore for small angles.

We now assume that grating bar tilt ϕ follows $\phi(x) = sx$, where x runs from -18 mm to + 18 mm for a grating with an active membrane of 36 mm in length. We vary the slope s. Therefore, a change of bar tilt by 0.01 deg/mm would lead to a bar tilt range of -0.18 deg to +0.18 deg over the entire grating.

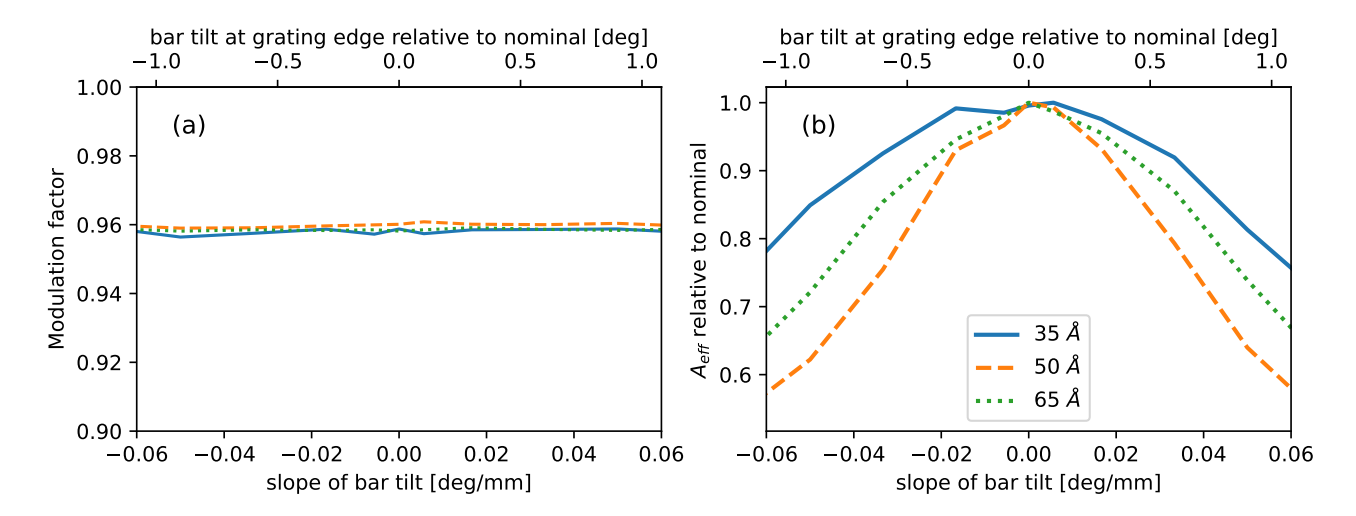


Figure 8: This figure shows how a bar tilt that changes with location on the grating influences the performance of REDSoX. Panel (a) shows the modulations factor that describes how much the signal from a polarized light source differs from the signal of an unpolarized light source. Panel (b) shows the impact on the effective area, scaled to the nominal performance of REDSoX.

The top scale in Fig. 8 shows the bar tilt at the edge of the grating in this model. The sign describes the change in bar tilt, i.e. whether it increases or decreases from left to right. The two panels in the figure display

the two crucial performance characteristics of REDSoX: The modulation factor, i.e. the ratio in signal expected from a polarized vs. an unpolarized source (panel (a)) and the effective area, i.e. the number of photons detected (panel (b)). Since the gratings do not change the polarization of the photons - they simply disperse the photons onto the LGMLs that are responsible for separating different polarization orientations - a change in the bar tilt has no effect in panel (a). However, the position of the gratings in REDSoX is chosen to maximize the number of photons diffracted in first order. If the bar tilt changes with position on the grating, then photons that do not hit the center of the grating (the gratings are mounted such that the center of the grating will have the nominal bar tilt), will encounter the bars at a different tilt than nominal, and thus more photons will end up in orders zero or two. Those photons will not hit the LGMLs in the correct location and thus will not contribute to the signal of a polarization measurement. The larger the slope of the bar tilt, the larger the fraction of photons that are not diffracted into order one will be, and thus the effective area is reduced compared to the nominal case of a bar tilt that is constant over the entire grating.

If we want to limit effective area losses to 10% or less, according to Fig. 6, we need bar tilt slope less than about ± 0.2 deg/mm, and ± 0.36 deg of tilt difference from the grating center. From Fig. 6 we predict that the grating etched as a chip meets this requirement only over a distance of about 24 mm, while the grating etched as a whole wafer meets this requirement everywhere.

6. EFFICIENCY MEASUREMENTS AT THE MIT POLARIMETRY BEAMLINE

Grating diffraction efficiency in the soft x-ray band is measured at the MIT x-ray polarimetry beamline.²⁴ It features a Manson electron-impact source with a variety of targets, a grating chamber centered about 8 m from the source, and a detector chamber another 2 m downstream. The x-ray source is mounted at 90 degrees relative to the rest of the beamline, and it illuminates an LGML at 45 degrees, which acts as a polarizer and narrow-band pass filter. Initially, a slit with 1 mm width along the long direction of the grating was used to illuminate the grating, integrating along the narrow direction.

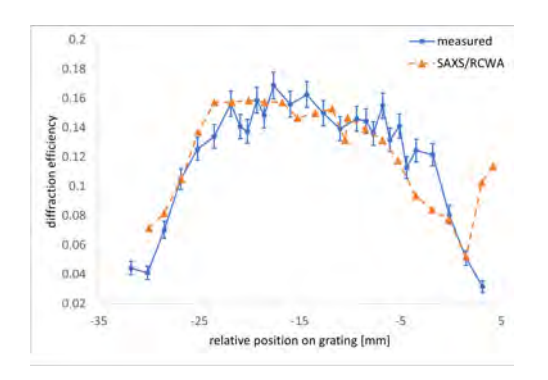
Each grating is measured separately. First, the grating is rocked in air around its axis parallel to the CAT grating bars until a laser beam coming from the source direction is reflected back onto itself. This establishes normal incidence onto the grating surface. After pumping down, the center of the grating is illuminated in the center with C-K x rays ($E \approx 0.28$ keV, $\lambda \approx 4.4$ nm), and an x-ray CCD measures the transmitted 1st order efficiency as a function of rocking angle. The grating is then rocked back to the angle where the 1st order efficiency peaked. A second scan then translates the grating perpendicular to the incident x rays, now measuring 1st order efficiency as a function of position along the long grating direction.

The left side of Fig. 9 compares 1st order diffraction efficiency x-ray data for grating FL13 with predictions from combining SAXS bar tilt data (Fig. 6) with a RCWA model prediction for 50 nm wide grating bars (Fig. 7). The agreement is fairly good, and the falloff towards both edges due to bar tilt variations is clearly visible. There can be a variety of reasons for discrepancies between SAXS/RCWA predictions and polarimetry beamline data. Our Cu-K SAXS data gives bar tilt (ideally) in the centers of about 20 hexagons every few mm along a line near the center of a grating, averaging over roughly $50 \times 50 \ \mu\text{m}^2$ at each location. Especially for samples deep etched as individual chips like FL13, the bar tilt along lines nearer to the edges of the sample could be significantly different from the measured line near the center. The measured bar tilt is then translated into diffraction efficiency at the grating rotation used in beamline measurements, using RCWA predictions for a specific bar geometry model. For these estimates we often pick simple bar geometry models, based on a small number of SEM images or from fitting beamline data to a zero-order rocking scan. In contrast, beamline measurements integrate over the whole width of the grating and over one to several mm along the long grating direction, depending on slit settings, using a slightly diverging C-K x-ray beam. (Later measurements were/are done without a slit, with the 1 inch wide CCD camera effectively acting as a wide slit. Efficiency as a function of position can simply be extracted from full-frame exposures.)

The right side of Fig. 9 compares first order efficiencies from gratings FL13 and FL15. The relatively flat bar tilt behavior of FL15 seen in Fig. 6 is reflected in the flat top shape of the x-ray data: efficiency is fairly constant across all 36 mm of the grating, with sharp drops at the L3 edges. However, the average efficiency is lower than for FL13. From SEM imaging we see that FL15 has bars close to 90 nm wide. A simple model would

predict a flat top near 14%, so this grating under-performs somewhat. Some reasons could be non-rectangular bar profiles, process tool contamination, or left-over residue from previous fabrication steps.

However, the limited budget of a sounding rocket mission does not allow us to try to diagnose each grating in depth. Instead, we decided that an average efficiency of 10% or higher across the full grating is considered sufficient for a flight grating, and no further investigation is required. Ref. 9 gives an overview of the x-ray characterization of all the gratings produced and measured so far.



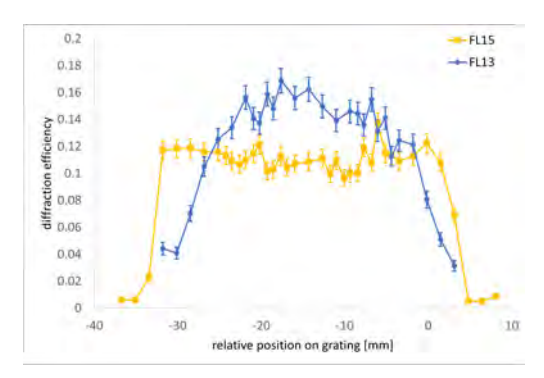


Figure 9: First order diffraction efficiency across a grating measured at C-K wavelength. Left: Data from grating FL13 ("measured"), compared to predictions based on SAXS data from Fig. 6 combined with the 50 nm-wide bar model from Fig. 7. The highest efficiency is observed along a roughly 24 mm wide region in accordance with SAXS/RCWA and ray tracing predictions. Right: Data from FL13 and FL15. See text for discussion.

7. CAT GRATING ROCKET FLIGHT





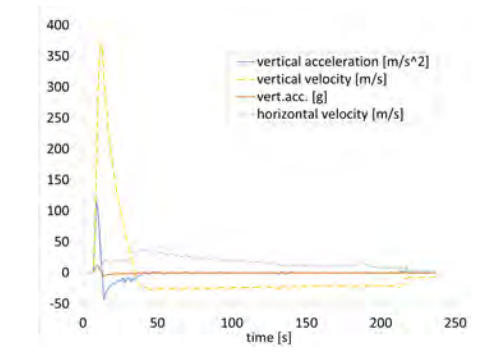


Figure 10: Left: Grating cassette taped to the underside of the electronics "sled" where the flight computers are mounted. Middle: Launch from Lake Winnipesaukee, NH. Right: Recorded flight parameters.

One of the authors (A. B.) is a hobby rocket builder. We decided to launch a CAT grating on one of his rocket flights. The rocket was 14 cm diameter and ≈ 2.4 meters tall with a liftoff weight of ≈ 18 kg. The motor was a solid fuel with a total impulse of $\approx 10,000$ Newton-seconds. The CAT grating was a witness sample from REDSoX production, $\approx 10 \times 30$ mm² in area, and mounted to a single wafer cassette via kapton tape on the corners. The cassette was mounted in the electronics bay of the rocket, which is vented to ambient air at all times. No environmental or mechanical protections were employed over the cassette. The rocket was launched from Lake Winnipesaukee, NH, on February 8, 2025. The winter was sufficiently cold to freeze the ice to allow people and small vehicles to safely transverse the ice. The weather on the launch day was sunny, ≈ -5 degrees C with scattered clouds and wind ≈ 3 meters per second at ground level. The rocket had two flight computers to control parachute deployments, a Marsa Systems 33L HD and an Altus Metrum "EasyMini", both of which reported

maximum altitude. Additionally, a Featherweight GPS Tracker transmitted and recorded real-time flight data over the long-range LoRa protocol. The flight reached a maximum acceleration of ≈ 12 g, a maximum speed of ≈ 370 m/s, and an apogee of ≈ 4330 m. A drogue parachute was deployed at apogee, reducing the descent rate to ≈ 25 m/s and a main parachute was deployed at 200 meters to achieve a landing speed of ≈ 7 m/s. The rocket was recovered ≈ 2 hours after launch and the grating was unmounted from the electronics bay after it was safely inside a temperature controlled room. Comparing SEM images from before and after the flight, no structural changes were detected, attesting to the ruggedness of CAT gratings.

While this was not a properly environmentally controlled vibration and thermal test with x-ray metrology, it was an easy and fun exercise to do at no cost to the project. Note that the launch and recovery of the rocket was a volunteer effort by A. B.

CAT gratings have been properly vibration and thermal vacuum tested before without any impact on performance. 9,25

8. LARGE-AREA CAT GRATINGS

Besides REDSoX work, we continue to improve deeper, larger ($\approx 32 \times 32 \text{ mm}^2$), and more efficient CAT gratings for potential future instruments and missions like Arcus^{8, 10, 11} or Lynx. ^{12, 26}

In this context we have recently measured diffraction efficiency for the first 5.7 μ m-deep CAT gratings made from 200 mm E-SOI wafers with reduced L1 widths. The measurements were performed at beamline 6.3.2 of the Advanced Light Source (ALS) at LBNL. The synchrotron beam diameter is smaller than the inside of an L2 hexagon, and it is centered within a hexagon during measurements. The beam averages over roughly 100 L1 cross support bars.

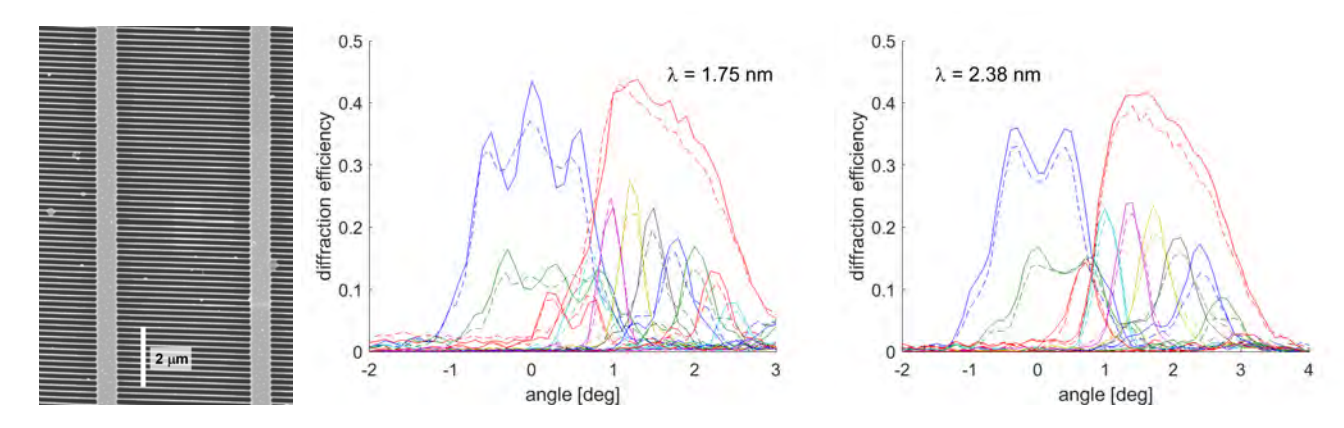


Figure 11: Left: Scanning electron micrograph of a bottom-up view of a 5.7 μ m-deep, 200 nm-period CAT grating, showing the narrow (~ 675 nm wide) L1 cross supports. Middle and Right: Measured diffraction efficiency as a function of incidence angle at 1.75 and 2.38 nm wavelengths, respectively. Dashed lines: Deep grating (SP3) with $\sim 1.1~\mu$ m-wide L1 supports after oxidation/HF thinning from References 8 and 27. Solid lines: Deep grating (S5) with narrow L1 supports as shown on the left. Blue lines: 0th order efficiency. Red lines: Sum over efficiency of blazed orders 3-11 ($\lambda = 1.75$ nm) or 3-9 ($\lambda = 2.38$ nm). L1 blockage is averaged over in the measurements, but there is no blockage from the L2 hexagon mesh.

The previous mask for OPL had been designed for 1.0 μ m-wide L1 cross supports. However, due to optical proximity effects the lithography resulted in 1.1 μ m-wide L1 bars. In the latest OPL mask for deep gratings we reduced the L1 width, and we now obtain roughly 600-700 nm wide L1 bars at the end of fabrication (see left of Fig. 11). This should result in a roughly 10% relative increase in throughput compared to gratings with wider L1 supports.

In Fig. 11 we compare diffraction efficiency of our most recent deep gratings with previous deep gratings with wider L1 bars that underwent additional, post-fabrication CAT grating bar thinning (reducing b in Fig. 1)

using repeated cycles of oxidation and oxide removal via vapor HF etching.^{8,27} The latter had been the highest efficiency CAT gratings produced to date, since the thinner grating bars typically lead to less blockage and increased throughput. As one can see, reducing the L1 bar widths leads to a further increase in efficiency in individual blazed orders. For the efficiency summed over the blazed orders we find relative increases in the range of roughly 6-14%, in line with expectations from the narrowing of L1 supports visible in SEM images. We plan to also subject some of these latest gratings to bar-thinning oxidation/vapor-HF-oxide-removal cycles, which should lead to even higher diffraction efficiencies.

9. DISCUSSION AND OUTLOOK

CAT gratings were chosen as the dispersive elements for the broad band soft x-ray polarimetry REDSoX mission. So far 43 gratings have been delivered, and another ~ 30 gratings are close to being finished. Production had started slowly and carefully, with initially lower yields, as we were figuring out how to best proceed in a quasi volume production mode. However, over the last six months we moved to larger batch sizes and higher yields. Most of the recent grating losses were singular events rather than systematic process issues. Gratings are handed off for efficiency measurements after optical and SEM inspection, and well over 90% of those gratings have cleared the efficiency cutoff. 9

The large majority of the delivered gratings have been made from wafers that were front side etched as full wafers. We found that even gratings from close to the wafer edge pass the acceptance test. Therefore, less than four wafers were required to provide all the gratings for REDSoX, and our backup plans to use local DRIE tools to etch chips on carrier wafers was not needed.

After acceptance, each gratings will be aligned in roll (rotation around the grating normal) to a slightly curved (to adjust for the converging x-ray beam) titanium mount with pitch/yaw flexures. Yaw (blaze) will later be adjusted based on the measured angle for best efficiency.

The front side DRIE step is a crucial step in determining the quality of the final CAT grating. The feedback used in this work to judge the DRIE outcome (SAXS, SEM imaging) is labor intensive, slow, destructive (cleaving for SEM cross sections), and often takes place many process steps after DRIE. We have recently obtained very encouraging results from Mueller matrix spectroscopic ellipsometry (MMSE) in combination with machine learning, which can be applied immediately after DRIE and is a fast and non-destructive metrology technique that supplies us with bar tilt²⁰ and bar profile data.²⁸ Such immediate in-line metrology is expected to accelerate process development and etch-recipe fine-tuning.

Future broadband soft x-ray polarimetry missions based on RESoX design modifications could feature higher spectral resolving power if they utilize higher CAT grating diffraction orders, and possibly higher effective area from utilizing multiple orders at once.

Producing a significant number of exchangeable CAT gratings for a flight mission within a reasonable, but limited time frame and low budget is a valuable exercise for future, more demanding flight instruments such as the proposed CAT grating spectrometers for Arcus and Lynx, which will need hundreds of CAT gratings of the highest quality, to be produced on a tight schedule. To guarantee a high probability of success under such conditions will require dedicated nanofabrication and metrology tool sets, a lengthy ramp-up period (tool orders and installs, personnel training, process development), and high process yields.

In the meantime we will continue to work on CAT grating efficiency improvements and increasing manufacturing readiness levels via fabrication process improvements.

ACKNOWLEDGMENTS

We thank J. Gregory, D. Young, and R. Lambert (MIT Lincoln Lab) for OPL and front side mask patterning of 200 mm SOI wafers. Special thanks to Charlie Settens and Jordan Cox (MIT) for speedy SAXSlab macros. This work was supported by NASA grants 80NSSC22K1904, 80NSSC23K0644, and 80NSSC24K1904, and by the MIT Kavli Institute for Astrophysics and Space Research. It was carried out in part through the use of MIT.nano's facilities. Some part of this work used resources of the Advanced Light Source, which is a DOE Office of Science User Facility under contract no. DE-AC02-05CH11231. The work was performed in part at

the Harvard University Center for Nanoscale Systems (CNS), and also at the Cornell NanoScale Facility (both members of the National Nanotechnology Coordinated Infrastructure Network (NNCI)), which both were - until recently, but not anymore - supported by the National Science Foundation under NSF award nos. ECCS-2025158 and NNCI-2025233, respectively.

REFERENCES

- [1] Marshall, H. L., Günther, H. M., Heilmann, R. K., Schulz, N. S., Egan, M., Hellickson, T., Heine, S. N. T., Windt, D. L., Gullikson, E. M., Ramsey, B., Tagliaferri, G., and Pareschi, G., "Design of a broadband soft xray polarimeter," *JOURNAL OF ASTRONOMICAL TELESCOPES INSTRUMENTS AND SYSTEMS* 4 (JAN 2018).
- [2] Soffitta, P., Baldini, L., Baumgartner, W., Bellazzini, R., Bongiorno, S. D., Bucciantini, N., Costa, E., Dovciak, M., Ehlert, S., Kaaret, P. E., Kolodziejczak, J. J., Latronico, L., Marin, F., Marscher, A. P., Marshall, H. L., Matt, G., Muleri, F., O'Dell, S. L., Poutanen, J., Ramsey, B., Romani, R. W., Slane, P., Tennant, A. F., Turolla, R., Weisskopf, M. C., Agudo, I., Antonelli, L. A., Bachetti, M., Bianchi, S., Bonino, R., Brez, A., Capitanio, F., Castellano, S., Cavazzuti, E., Chen, C.-T., Ciprini, S., Cocchi, M., Churazov, E., De Rosa, A., Del Monte, E., Di Gesu, L., Di Lalla, N., Di Marco, A., Donnarumma, I., Doroshenko, V., Enoto, T., Evangelista, Y., Fabiani, S., Ferrazzoli, R., Garcia, J. A., Gunji, S., Heyl, J., Ingram, A., Iwakiri, W., Jorstad, S. G., Karas, V., Kaspi, V., Kislat, F., Kitaguchi, T., Krawczynski, H., La Monaca, F., Liodakis, I., Madejski, G., Maldera, S., Manfreda, A., Marinucci, A., Massaro, F., Mitsuishi, I., Mizuno, T., Negro, M., Ng, S., Omodei, N., Oppedisano, C., Papitto, A., Pavlov, G. G., Perri, M., Pesce-Rollins, M., Petrucci, P.-O., Pilia, M., Possenti, A., Puccetti, S., Rankin, J., Ratheesh, A., Roberts, O. J., Sgro, C., Spandre, G., Stella, L., Sunyaev, R., Swartz, D. A., Tamagawa, T., Tavecchio, F., Taverna, R., Tawara, Y., Thomas, N. E., Tombesi, F., Trois, A., Tsygankov, S. S., Vink, J., Wu, K., Xie, F., and Zane, S., "The Imaging X-ray Polarimetry Explorer 2.5 years later," in [SPACE TELESCOPES AND INSTRUMENTATION 2024: ULTRAVIOLET TO GAMMA RAY, PT 1], DenHerder, J., Nikzad, S., and Nakazawa, K., eds., Proceedings of SPIE 13093 (2024). Conference on Space Telescopes and Instrumentation - Ultraviolet to Gamma Ray, Yokohama, JAPAN, JUN 16-21, 2024.
- [3] Marshall, H., Heine, S., Garner, A., Masterson, R., Günther, M., Heilmann, R. K., Bongiorno, S., and Gullikson, E., "The Rocket Experiment Demonstration of a Soft X-ray Polarimeter (REDSoX)," PoS MULTIF2023, 076 (2024).
- [4] Bongiorno, S. D., "Full-shell replicated x-ray optics modules for REDSoX and FOXSI-5," these proceedings (2025).
- [5] Günther, H. M., Egan, M., Heilmann, R. K., Heine, S. N. T., Hellickson, T., Frost, J., Marshell, H. L., Schulz, N. S., and Theriault-Shay, A., "REDSoX: Monte-Carlo ray-tracing for a soft x-ray spectroscopy polarimeter," in [OPTICS FOR EUV, X-RAY, AND GAMMA-RAY ASTRONOMY VIII], ODell, S. and Pareschi, G., eds., Proceedings of SPIE 10399, SPIE (2017). Conference on Optics for EUV, X-Ray, and Gamma-Ray Astronomy VIII, San Diego, CA, AUG 08-10, 2017.
- [6] Heilmann, R. K., Huenemoerder, D. P., McCoy, J. A., and McEntaffer, R. L., "Diffraction gratings for x-ray spectroscopy," https://arxiv.org/abs/2409.02297 (2024).
- [7] Canizares, C., Davis, J., Dewey, D., Flanagan, K., Galton, E., Huenemoerder, D., Ishibashi, K., Markert, T., Marshall, H., McGuirk, M., Schattenburg, M., Schulz, N., Smith, H., and Wise, M., "The Chandra high-energy transmission grating: Design, fabrication, ground calibration, and 5 years in flight," PUBLICATIONS OF THE ASTRONOMICAL SOCIETY OF THE PACIFIC 117, 1144-1171 (OCT 2005).
- [8] Heilmann, R. K., Bruccoleri, A. R., Gregory, J. A., Gullikson, E. M., Günther, H. M., Hertz, E., Lambert, R. D., Young, D. J., and Schattenburg, M. L., "Transmission grating arrays for the x-ray spectrometer on Arcus Probe," submitted to JOURNAL OF ASTRONOMICAL TELESCOPES INSTRUMENTS AND SYSTEMS (2024).
- [9] Heine, S. N. T., Marshall, H. L., Garner, A., Angile, E., Baker, C. M., Heilmann, R. K., Juneau, J., and Ravia, S., "Mission design and development of the rocket experiment demonstration of a soft x-ray (REDSoX) polarimeter," to be published in Proc. SPIE **13625** (2025).

- [10] Smith, R. K., Bautz, M., Bregman, J., Brenneman, L., Brickhouse, N., Bulbul, E., Burwitz, V., Bushman, J., Canizares, C., Chakrabarty, D., Cheimets, P., Costantini, E., DeRoo, C., Falcone, A., Foster, A., Gallo, L., Grant, C., Günther, H. M., Heilmann, R. K., Heine, S., Hine, B., Huenemoerder, D., Jara, S., Kaastra, J., Kara, E., Kreykenbohm, I., Madsen, K., Marshall, H., McDonald, M., McEntaffer, R., Miller, J., Miller, E., Mushotzky, R., Nandra, K., Nowak, M., Paerels, F., Petre, R., Poppenhaeger, K., Ptak, A., Reid, P., Ronzano, K., Rozanska, A., Samra, J., Sanders, J., Schattenburg, M., Schonfeld, J., Schulz, N., Smale, A., Temi, P., Valencic, L., Walker, S., Wilms, J., and Wolk, S., "Arcus: exploring the formation and evolution of clusters, galaxies, and stars," in [Space Telescopes and Instrumentation 2022: Ultraviolet to Gamma Ray], den Herder, J.-W. A., Nikzad, S., and Nakazawa, K., eds., 12181, 1218121, International Society for Optics and Photonics, SPIE (2022).
- [11] Smith, R. K., "The Arcus Probe mission," in [UV, X-Ray, and Gamma-Ray Space Instrumentation for Astronomy XXIII], 12678, International Society for Optics and Photonics, SPIE (2023).
- [12] Günther, H. M. and Heilmann, R. K., "Lynx soft x-ray critical-angle transmission grating spectrometer," JOURNAL OF ASTRONOMICAL TELESCOPES INSTRUMENTS AND SYSTEMS 5 (APR 2019).
- [13] Bruccoleri, A., Guan, D., Mukherjee, P., Heilmann, R. K., Schattenburg, M. L., and Vargo, S., "Potassium hydroxide polishing of nanoscale deep reactive-ion etched ultrahigh aspect ratio gratings," *JOURNAL OF VACUUM SCIENCE & TECHNOLOGY B* 31 (NOV 2013).
- [14] Heilmann, R. K., Bruccoleri, A. R., Song, J., Levenson, B., Smallshaw, B., Whalen, M., Garner, A., Heine, S. T., Marshall, H. L., Cook, M. T., Gregory, J. A., Lambert, R. D., Shapiro, D. A., Young, D. J., Gullikson, E. M., Nonaka, T., Uchida, A., Quijada, M. A., Hertz, E., Cheimets, P., Smith, R. K., and Schattenburg, M. L., "Manufacture and performance of blazed soft x-ray transmission gratings for Arcus and Lynx," in [OPTICS FOR EUV, X-RAY, AND GAMMA-RAY ASTRONOMY X], ODell, S., Gaskin, J., and Pareschi, G., eds., Proceedings of SPIE 11822, SPIE (2021). Conference on Optics for EUV, X-Ray, and Gamma-Ray Astronomy X, San Diego, CA, AUG 01-05, 2021.
- [15] Bruccoleri, A. R., Guan, D., Heilmann, R. K., Vargo, S., DiPiazza, F., and Schattenburg, M. L., "Nanofabrication advances for high efficiency critical-angle transmission gratings," in [OPTICS FOR EUV, X-RAY, AND GAMMA-RAY ASTRONOMY VI], ODell, S. and Pareschi, G., eds., Proceedings of SPIE 8861, SPIE (2013). Conference on Optics for EUV, X-Ray, and Gamma-Ray Astronomy VI as part of the SPIE Optics + Photonics International Symposium on Optical Engineering + Applications, San Diego, CA, AUG 26-29, 2013.
- [16] Bruccoleri, A. R., Heilmann, R. K., and Schattenburg, M. L., "Fabrication process for 200 nm-pitch polished freestanding ultrahigh aspect ratio gratings," JOURNAL OF VACUUM SCIENCE & TECHNOLOGY B 34 (NOV-DEC 2016).
- [17] Heilmann, R. K., Bruccoleri, A. R., Song, J., Cook, M. T., Gregory, J. A., Lambert, R. D., Shapiro, D. A., Young, D. J., Bradshaw, M., Burwitz, V., Hartner, G. D., Langmeier, A., Smith, R. K., and Schattenburg, M. L., "Toward volume manufacturing of high-performance soft x-ray critical-angle transmission gratings," in [SPACE TELESCOPES AND INSTRUMENTATION 2020: ULTRAVIOLET TO GAMMA RAY], Den-Herder, J., Nikzad, S., and Nakazawa, K., eds., Proceedings of SPIE 11444, SPIE (2021). Conference on Space Telescopes and Instrumentation Ultraviolet to Gamma Ray / SPIE Astronomical Telescopes + Instrumentation Conference, DEC 14-18, 2020.
- [18] Heilmann, R. K., Bruccoleri, A. R., Gullikson, E. M., Smith, R. K., and Schattenburg, M. L., "Soft x-ray performance and fabrication of flight-like blazed transmission gratings for the x-ray spectrometer on Arcus Probe," in [Optics for EUV, X-Ray, and Gamma-Ray Astronomy XI], O'Dell, S. L., Gaskin, J. A., Pareschi, G., and Spiga, D., eds., 12679, 126790L, International Society for Optics and Photonics, SPIE (2023).
- [19] Heilmann, R. K., Bruccoleri, A. R., Burwitz, V., deRoo, C., Garner, A., Günther, H. M., Gullikson, E. M., Hartner, G., Hertz, E., Langmeier, A., Müller, T., Rukdee, S., Schmidt, T., Smith, R. K., and Schattenburg, M. L., "X-ray performance of critical-angle transmission grating prototypes for the Arcus mission," ASTROPHYSICAL JOURNAL 934 (2022).
- [20] Mudide, S., Keller, N., Andrew Antonelli, G., Cruz, G., Hart, J., Bruccoleri, A. R., Heilmann, R. K., and Schattenburg, M. L., "Machine learning driven measurement of high-aspect-ratio nanostructures using Mueller matrix spectroscopic ellipsometry," *Journal of Vacuum Science Technology B* 43, 012801 (01 2025).

- [21] Song, J., Heilmann, R. K., Bruccoleri, A. R., and Schattenburg, M. L., "Characterizing profile tilt of nanoscale deep-etched gratings via x-ray diffraction," *JOURNAL OF VACUUM SCIENCE & TECHNOL-OGY B* 37 (NOV 2019).
- [22] Moharam, M., Pommet, D., Grann, E., and Gaylord, T., "Stable implementation of the rigorous coupled-wave analysis for surface-relief gratings enhanced transmittance matrix approach," JOURNAL OF THE OPTICAL SOCIETY OF AMERICA A-OPTICS IMAGE SCIENCE AND VISION 12, 1077–1086 (MAY 1995). Optical-Society-of-America 2nd Topical Meeting on Diffractive Optics, ROCHESTER, NY, JUN 06-09, 1994.
- [23] Heilmann, R. K., Bruccoleri, A. R., Song, J., and Schattenburg, M. L., "Progress in x-ray critical-angle transmission grating technology development," in [OPTICS FOR EUV, X-RAY, AND GAMMA-RAY AS-TRONOMY IX], ODell, S. and Pareschi, G., eds., Proceedings of SPIE 11119, SPIE (2019). Conference on Optics for EUV, X-Ray, and Gamma-Ray Astronomy IX as part of the SPIE Optics + Photonics International Symposium on Optical Engineering + Applications, San Diego, CA, AUG 13-15, 2019.
- [24] Garner, A., Marshall, H. L., Heine, S. N. T., Heilmann, R. K., Song, J., Schulz, N. S., LaMarr, B. J., and Egan, M., "CAT grating alignment and testing for soft x-ray polarimetry," in [SPACE TELESCOPES AND INSTRUMENTATION 2020: ULTRAVIOLET TO GAMMA RAY], DenHerder, J., Nikzad, S., and Nakazawa, K., eds., Proceedings of SPIE 11444, SPIE (2021). Conference on Space Telescopes and Instrumentation Ultraviolet to Gamma Ray / SPIE Astronomical Telescopes + Instrumentation Conference, DEC 14-18, 2020.
- [25] Heilmann, R. K., Bruccoleri, A. R., Song, J., Kolodziejczak, J., Gaskin, J. A., O'Dell, S. L., Cheimetz, P., Hertz, E., Smith, R. K., Burwitz, V., Hartner, G., La Caria, M.-M., and Schattenburg, M. L., "Critical-angle transmission grating technology development for high resolving power soft x-ray spectrometers on Arcus and Lynx," in [OPTICS FOR EUV, X-RAY, AND GAMMA-RAY ASTRONOMY VIII], ODell, S. and Pareschi, G., eds., Proceedings of SPIE 10399, SPIE (2017). Conference on Optics for EUV, X-Ray, and Gamma-Ray Astronomy VIII, San Diego, CA, AUG 08-10, 2017.
- [26] Gaskin, J. A., Swartz, D. A., Vikhlinin, A., Ozel, F., Gelmis, K. E., Arenberg, J. W., Bandler, S. R., Bautz, M. W., Civitani, M. M., Dominguez, A., Eckart, M. E., Falcone, A. D., Figueroa-Feliciano, E., Freeman, M. D., Günther, H. M., Havey, K. A., Heilmann, R. K., Kilaru, K., Kraft, R. P., McCarley, K. S., McEntaffer, R. L., Pareschi, G., Purcell, W., Reid, P. B., Schattenburg, M. L., Schwartz, D. A., Schwartz, E. D., Tananbaum, H. D., Tremblay, G. R., Zhang, W. W., and Zuhone, J. A., "Lynx x-ray observatory: an overview," JOURNAL OF ASTRONOMICAL TELESCOPES INSTRUMENTS AND SYSTEMS 5 (APR 2019).
- [27] Heilmann, R. K., Bruccoleri, A. R., Gullikson, E. M., Günther, H. M., Smith, R. K., and Schattenburg, M. L., "Improved efficiency critical-angle transmission gratings for high-resolution soft x-ray spectroscopy," in [Space Telescopes and Instrumentation 2024: Ultraviolet to Gamma Ray], den Herder, J.-W. A., Nikzad, S., and Nakazawa, K., eds., 13093, 1309313, International Society for Optics and Photonics, SPIE (2024).
- [28] Mudide, S., "Deep learning outperforms RCWA for multimodal measurement of high-aspect-ratio nanostructures," paper in progress.